Hexagonal pattern instabilities in rotating Rayleigh-Bénard convection of a non-Boussinesq fluid: Experimental results

Alessio Guarino, Valerie Vidal

PHYSICAL REVIEW E **69**, 066311 (2004)

Hexagonal pattern instabilities in rotating Rayleigh-Bénard convection of a non-Boussinesq fluid: Experimental results

Alessio Guarino*
iQuest, University of California Santa Barbara, Santa Barbara, 93106 California, USA

Valerie Vidal†
Institut de Physique du Globe de Paris, 4 Place Jussieu, 75252 Paris Cedex 05, France

(Received 2 January 2004; revised manuscript received 2 March 2004; published 16 June 2004)

Motivated by the Küppers-Lortz instability of roll patterns in the presence of rotation, we have investigated the effects of rotation on a hexagonal pattern in Rayleigh-Bénard convection. While several theoretical models have been developed, experimental data cannot be found in the literature. In order to check the validity of the predictions and to study the effects of rotation on the behavior of the system, we present experimental results for a non-Boussinesq Rayleigh-Bénard convection with rotation about the vertical axis. Rotation introduces an additional control parameter, namely the dimensionless rotation rate $\Omega = 2\pi f d^2/\nu$, where f is the rotation rate (in Hz), d is the thickness of the cell, and ν is the kinematic viscosity. We observe that the cell rotation induces a slow rotation of the pattern in the opposite direction ($\approx \Omega \times 10^{-4}$) in the rotating frame. Moreover, it tends to destroy the convective pattern. No oscillation of the hexagonal pattern over the range of its existence ($\Omega \leqslant 6$) has been observed.

DOI: 10.1103/PhysRevE.69.066311 PACS number(s): 47.54.+r, 47.27.Te, 47.20.Ky

I. INTRODUCTION

Experiments allowing a quantitative comparison with theoretical investigations are essential to check available theories and to suggest new directions in theoretical studies. This has been particularly successful for Rayleigh-Bénard convection: the convective system consisting of a thin, wide horizontal fluid layer confined between two parallel rigid plates and heated from below has become a paradigm of pattern formation [1–3].

A fluid is non-Boussinesq when the dependence of its properties on temperature is not negligible [4,5]. Theory [6–11] predicts that in a non-Boussinesq Rayleigh-Bénard convection, hexagons are formed via a subcritical bifurcation when the Rayleigh number R, which is proportional to the temperature difference ΔT between the bottom and the top plate, increases above its critical value R_c (i.e., $\Delta T > \Delta T_c$). In terms of the adimensional parameter $\varepsilon = \Delta T/\Delta T_c - 1$, the bifurcation diagram shows that hexagons are stable for $\varepsilon_a < \varepsilon < \varepsilon_b$ and rolls are stable for $\varepsilon > \varepsilon_r$ (Fig. 1). Previous experiments confirmed the validity of those theoretical predictions [12–18]. However, the effect on a convective non-Boussinesq fluid of a rotation about a vertical axis has still not been experimentally investigated, while several theoretical models have been developed. Motivated by the Küppers-Lortz instability of roll patterns in the presence of rotation, we have investigated experimentally the effects of rotation on a hexagonal convective pattern. Rotation breaks the up-down symmetry and introduces an additional control parameter, namely the dimensionless rotation rate $\Omega = 2\pi f d^2/\nu$, where f is the rotation rate (in Hz), d is the thickness of the cell, and ν is the kinematic viscosity [19,20]. Theory [20–24] agrees in predicting that in the presence of rotation, the hexagonal pattern is still the primary instability. Disagreement is over the secondary instability, i.e., what happens when one keeps increasing the control parameter ε. Some [20–22] predict that the steady hexagons lead to oscillating hexagons via a Hopf bifurcation when $\Omega > \Omega_{KL}$, where Ω_{KL} is the rotation rate above which the Küppers-Lortz instability is predicted [19]. Others [23,24] predict that, in the presence of rotation, the steady hexagons go to modulated (in space and time) hexagons via a supercritical bifurcation. They also predict that if one keeps increasing ε, the modulated hexagons themselves become unstable and a regular pattern breaks down, leading to a temporally and spatially chaotic state. In this case, the disordered state locally exhibits a structure with hexagonal symmetry which rotates in time.

In order to check which one of these theories predicts the real behavior of the system, we have performed some experiments of Rayleigh-Bénard convection on a non-Boussinesq fluid (SF_6) with rotation about the vertical axis. The results are compared to the theoretical predictions and help to gain a better understanding of the consequences of rotation on the system behavior.

II. APPARATUS AND EXPERIMENTAL PROCEDURE

All experiments have been performed in a Rayleigh-Bénard convection cell with a circular cross section of radius $r = 4.17 \pm 0.005$ cm, rotating around the vertical axis. A detailed description for the experimental setup can be found in [25]. The fluid (gas) is SF_6 at a pressure of 107.839 ± 0.001 psi; the Prandtl number σ is 0.797. The top plate is a sapphire and the bottom plate is an optical flat diamond-machined aluminum surface [26]. We have used a

*Currently at Université de la Polynésie Française, Tahiti, French Polynesia. Electronic address: guarino@upf.pf
†Electronic address: vidal@ipgp.jussieu.fr

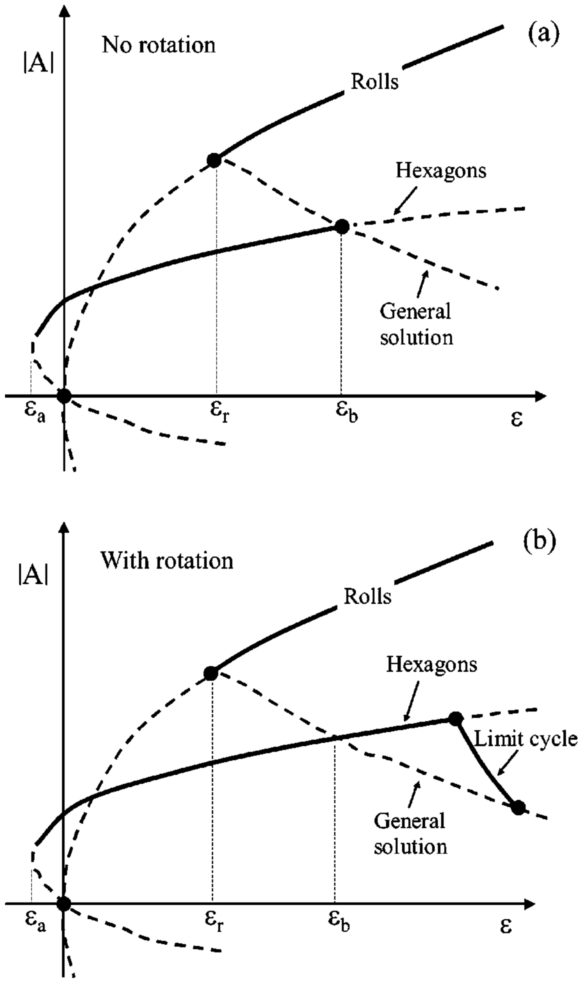

FIG. 1. Bifurcation diagram for a non-Boussinesq fluid [23]. Without rotation (a) the hexagons gain stability through a saddle node bifurcation. Hexagons are stable for $\varepsilon_a < \varepsilon < \varepsilon_b$ and rolls are stable for $\varepsilon > \varepsilon_r$. Hexagons become unstable through a transcritical bifurcation involving a general solution, where the three amplitudes are all nonzero but not all equal. $|A|$ is the amplitude of the instability. With rotation (b), the hexagons become unstable to a limit cycle through a Hopf bifurcation (oscillating hexagons). The limit cycle terminates at the general solution branch.

paper sidewall. The spacing d between the two plates is 710 ± 1 μm, corresponding to an aspect ratio $\Gamma = r/d = 58.80 \pm 0.15$. The mean temperature of the fluid has been fixed at $T = 40$ °C. In these conditions, for $\Omega = 0$, we expect a temperature difference $\Delta T_c = 18.99$ °C for the onset of the convective regime (from $R = \alpha g d^3 \Delta T / \kappa \nu = 1708$, where α is the coefficient of thermal expansion, g is the acceleration of gravity, and κ is the thermal diffusivity). The vertical thermal diffusion time is $t_\nu = d^2/\kappa = 1.121$ s, $\varepsilon_a = -5.17 \times 10^{-4}$, $\varepsilon_r = 0.016$, and $\varepsilon_b = 0.0613$. Shadowgraph visualization has been used to image the system [25]. The camera, set in the rotating frame, takes images of the cell from above. The distance between the pixels is 263 ± 1 μm. For each experiment, first Ω is imposed to the system, and then the temperature difference ΔT (given ε). We then wait 1.5 h ($\simeq 4817 t_\nu$) in order to let the top and bottom plates' temperatures equilibrate. Then we take 256, 512, or 912 pictures. The elapsed time δt between two consecutive images varies between 0.39 and 300 s.

The working parameters such as the cell thickness, the pressure, and the mean temperature have been optimized to fit the apparatus characteristics and limitations. The best compromise has been found in order to have, at the same time, the best shadowgraph sensitivity, the greatest aspect ratio Γ, the largest existence domain for the hexagons and $\Delta T_{\mathrm{rolls}} < \Delta T_{\max} \simeq 30$ °C, where $\Delta T_{\mathrm{rolls}}$ is the temperature difference at which the rolls are stable and $\Delta T_{\max}$ is the largest temperature difference which is possible to apply to the system.

In order to check the effects of the boundary conditions on the convective pattern, similar experiments have been performed on a Rayleigh-Bénard convection cell with smoother boundary conditions on the bottom plate (ramp). For this cell, the spacing d_0 between the top plate and the flat part of the bottom plate ($0 \leq r \leq r_0 = 3.18$ cm) is 760 ± 1 μm, corresponding to $\Gamma_0 = r_0/d_0 = 42.6 \pm 0.15$. Over the radius interval $r_0 < r < r_1 = 4.44$ cm, the bottom plate has a profile yielding $d/d_0 = 1 - 0.036[1 - \cos\{(r - r_0)\pi/(r_1 - r_0)\}]$. The mean temperature and the pressure of the fluid are the same as that in the flat bottom plate cell.

III. RESULTS

At $\Omega = 0$, the temperature difference for the onset of convection is $\Delta T_c = 18.73$ °C, measured by shadowgraphy. In Fig. 2, images of the flat cell are shown at $\varepsilon = 0.01$, 0.02, and 0.03 for different values of Ω. They are obtained by image processing of the direct shadowgraph visualization. First, the raw pictures are divided by a background image, taken at $\varepsilon < 0$, in order to eliminate the dependence of the illumination or the bottom plate reflectivity on the local heterogeneities. After performing a two-dimensional fast Fourier transform (FFT), a radial filter is applied. An inverse FFT then leads to the final image. More details on this procedure are developed in [25]. For $\Omega = 0$ [Figs. 2(a), 2(e), 2(i), 3(a), and 3(c)], the primary instability consists of a hexagonal pattern ($\varepsilon \leq 0.02$), evolving towards a straight roll pattern for larger ε.

When a rotation about the vertical axis is imposed on the system, two main effects can be observed. The first one is the appearance of randomly distributed defects in the hexagonal pattern. Those defects consist mostly of small domains in which a roll pattern develops. These small roll patterns can be seen at low $\Omega(\leq 4)$ and at $\varepsilon \leq 0.02$ [see Figs. 2(b), 2(c), 2(f), and 2(g)]. The number of those defects depends on ε and is independent of Ω. The second effect due to the rotation is the invasion, from the edge of the cell towards the center, of three different oriented sets of rolls. As Ω increases, these three sets of rolls appear at a lower ε. The interval in ε in which the hexagonal pattern and then the rolls predicted for $\Omega = 0$ (for larger ε) are observed thus becomes smaller for larger rotation rates. For $3 \leq \Omega \leq 6$, these rolls never develop and the system switches directly from hexagons to three sets of rolls [Figs. 2(k), 2(l), 3(b), and 3(d)]. For $\Omega \geq 6$, the hexagonal pattern is never observed [Figs. 2(d), 2(h), and 2(l)]. Therefore, the domain in Ω shows an

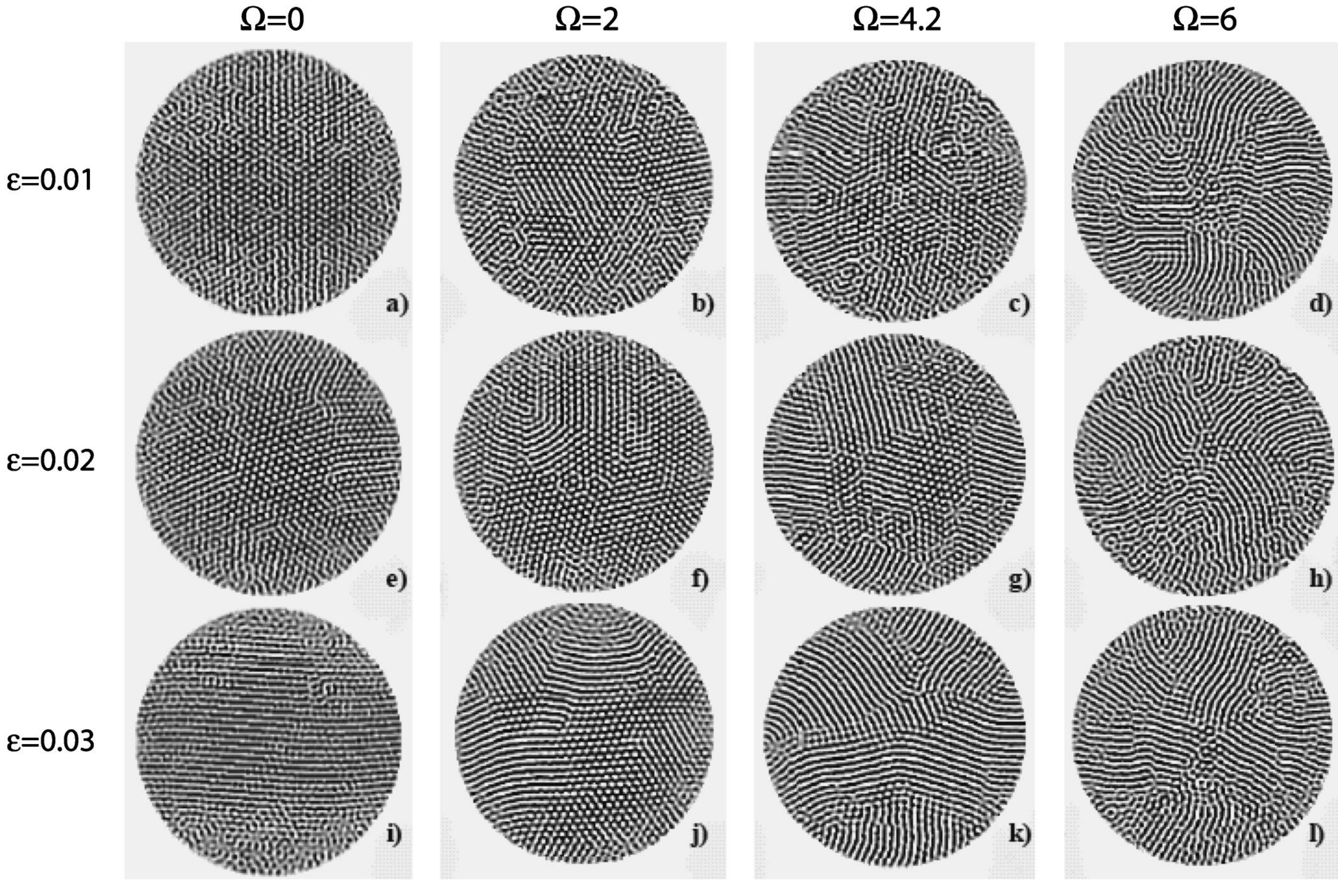

FIG. 2. Images of the convective pattern in the flat cell (observed from above). $\varepsilon=0.01$, 0.02, and 0.03 for the first (a,b,c,d), second (e,f,g,h), and third row (i,j,k,l), respectively. $\Omega=0$, 2, 4.2, and 6 for the first (a,e,i), second (b,f,j), third (c,g,k), and fourth column (d,h,l), respectively. The image processing required to obtain these pictures is described in the text.

upper limit for the developing and thus the analysis of the hexagonal pattern. All these results are summarized in Fig. 4, where the region of stability in the (ε,Ω) plane is indicated for each observed pattern.

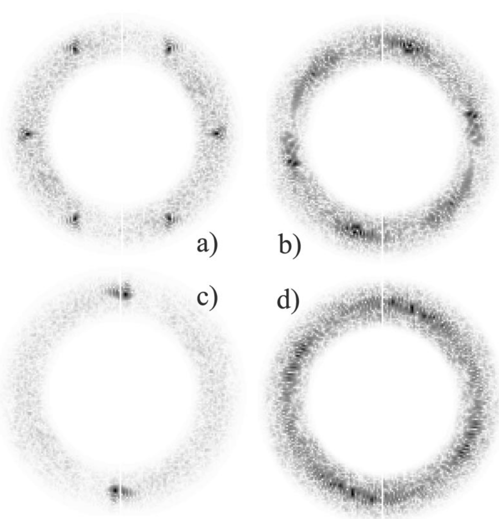

FIG. 3. (a,b,c,d) show the calculated structure functions $S(\vec{k},t)$ of images (e,g,i,l) from Fig. 2, respectively (see text). In (a), the six characteristic peaks of a hexagonal pattern can be observed, while (c) shows the two characteristic peaks of a roll pattern.

In order to characterize the hexagonal pattern, we have computed the structure factor $S(\vec{k},t)$, defined as the modulus of the two-dimensional FFT (Fig. 3). To study the dynamics of the three sets of rolls composing the hexagonal pattern, we have first calculated the angular distribution $F(\theta,t)$ $(0<\theta<\pi)$, where $F(\theta,t)$ is the integral of $S(\vec{k},t)$ over k in the upper half-plane $k_y>0$ [Fig. 5(a)]. We then calculate the integral of the peaks (maxima) I_i $(i=1,2,3)$, corresponding to the three sets of rolls composing the hexagonal structure. The behavior of I_i $(i=1,2,3)$ as a function of time is then studied [Figs. 6 and 5(b)]. Because the edge mode tends to destroy the hexagonal pattern, only the central part of the cell (40% of the radius) has been considered. In order to check a large range of frequencies (between 10^{-5} and 1.3 Hz), different sampling times δt, i.e., the time elapsed between two consecutive pictures, have been used $(0.3<\delta t<300$ s). The three peaks always have about the same amplitude, and no periodicity is found in the behavior of the amplitudes. As an example, in Fig. 6 the I_i $(i=1,2,3)$ are plotted as a function of time for $\Omega=3$ and $\varepsilon=0.003$. In Figs. 6(a), 6(c), and 6(e), $\delta t=200$ s, while in Figs.

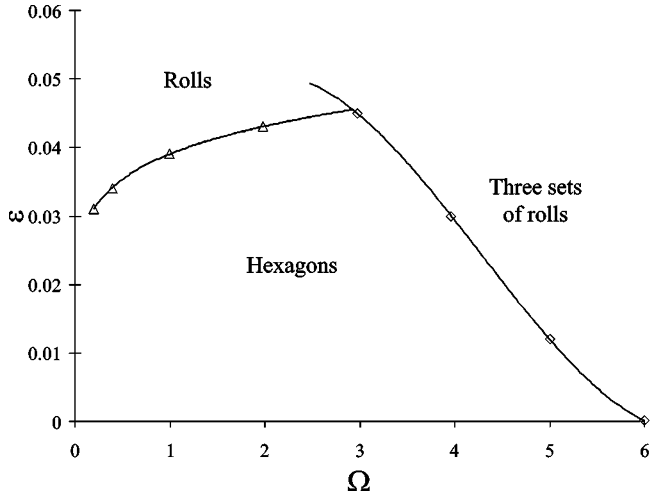

FIG. 4. Experimental phase diagram. The region of stability of the different observed patterns is represented in the (ε,Ω) plane. At low rotation rate $(\Omega<3)$, the system goes from hexagons to rolls. For $3\leqslant\Omega\leqslant 6$, rolls never develop and the system switches from hexagons to three sets of rolls. At high rotation rate $(\Omega>6)$, the three sets of rolls become the primary instability.

6(b), 6(d), and 6(f), $\delta t=0.39$ s. The I_i's temporal Fourier transforms [Figs. 6(g) and 6(h)] show that there is no periodicity in their behavior. Similar results have been found for all the Ω and ε at which the hexagonal pattern is formed.

Figure 5(b) shows a typical time plot of the angular distribution $F(\theta,t)$ when the hexagonal pattern is present, for $\delta t=22.89$ s, $\Omega=2$, and $\varepsilon=0.017$. The position of the maxima changes as a function of time. Their velocity is constant and it can be calculated by determining the position of the maximum at each time. That means that there is a periodic rotation, at frequency f_p ($\omega=2\pi f_p d^2/\nu$, in term of adimensional frequency) of the two-dimensional Fourier transform. This rotation is opposite to the cell one, i.e., the fluid rotates slower than the whole apparatus (note that the images are taken in the rotating frame). The value of ω is about 10^3–10^4 times smaller than Ω.

In Fig. 7, the dimensionless rotation rate ω of the Fourier transform has been plotted as a function of ε for different values of Ω. Measurements have been made at $\Omega=2$ (diamonds), $\Omega=3$ (squares), $\Omega=4.2$ (open circles), and $\Omega=5$ (triangles). The lines indicate the best linear fit $\omega=a_\Omega\varepsilon$. For each Ω, in the limit of the experimental errors, the fits indicate that for $\varepsilon=0$, $\omega=0$. Therefore, at the onset of convection, the fluid has the same angular velocity as the cell. The plot in Fig. 8 shows the linear relationship between the coefficient a_Ω and Ω^3. This confirms the logical assumption that ω depends both on the modulus and on the direction of Ω. The plot of ω as a function of $\varepsilon\Omega^3$ (Fig. 9) shows that all points represented in Fig. 7 collapse together on a straight line. We can therefore conclude that $\omega=c\varepsilon\Omega^3$, and we find $c=4.6\times 10^{-4}$. Within the limit of the experimental errors, $\omega=0$ at the onset of convection.

The results of the experiments performed with a ramp on the bottom plate of the cell are similar to those obtained with

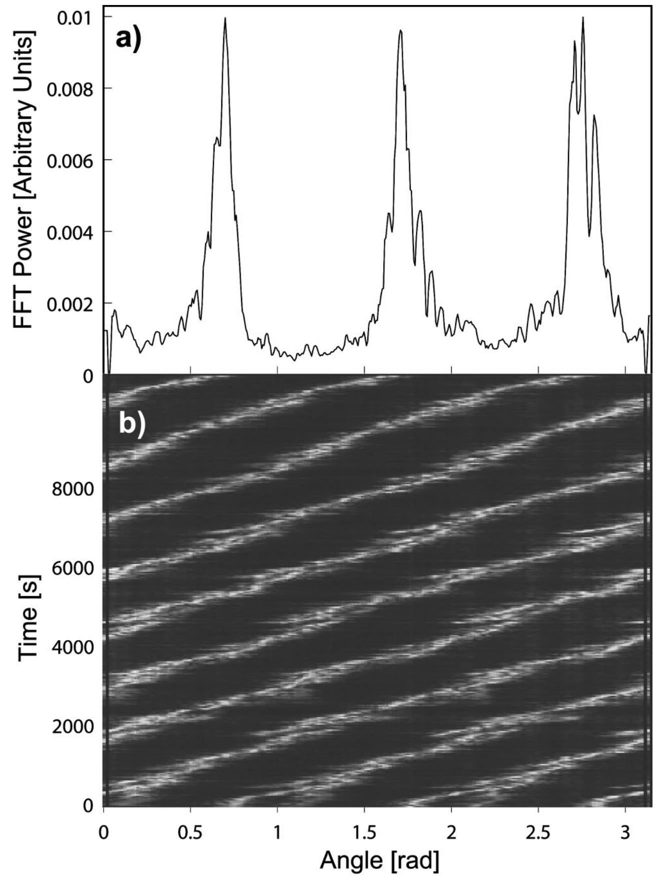

FIG. 5. (a) Angular distribution $F(\theta,t)$ as a function of θ for the hexagonal pattern found at $\varepsilon=0.017,\Omega=2$. The three peaks represent the three sets of rolls composing the hexagonal structure which are 60° apart. $F(\theta,t)$ is normalized so that $\int F(\theta,t)\,d\theta=1$. The $F(\theta,t)$ plotted here is the first of the series shown in the time-angle plot below. (b) Time-angle plot for the same experiment. Images are taken with a $\delta t=22.89$ s time interval. The 2D Fourier transform rotates with a period of 75 507 s, corresponding to a dimensionless $\omega=10^{-4}$.

the flat cell. Indeed, we have observed a periodic rotation of the two-dimensional Fourier transform. Once again, no oscillating hexagons have been observed. The effects of rotation on the convective pattern are the same as in the previous set of experiments. The only difference is that in the cell with the ramp, the rolls are not straight but curved (Fig. 10). Then their two-dimensional Fourier transform does not consist of a small circular spot, but of a comma-shaped spot (Fig. 10). The solid circles in Fig. 9 represent the measurements made with the cosinusoidal-ramp-shaped cell at $\Omega=3.93$. The best linear fit for those points is the same, in the limit of the experimental errors, as the one fitting the measurements made with the flat cell.

IV. CONCLUSION

Our experiments in Rayleigh-Bénard convection with rotation about the vertical axis have shown no oscillating hexagonal pattern. Instead, we have observed two different features in the rotating cell. First, small localized defects

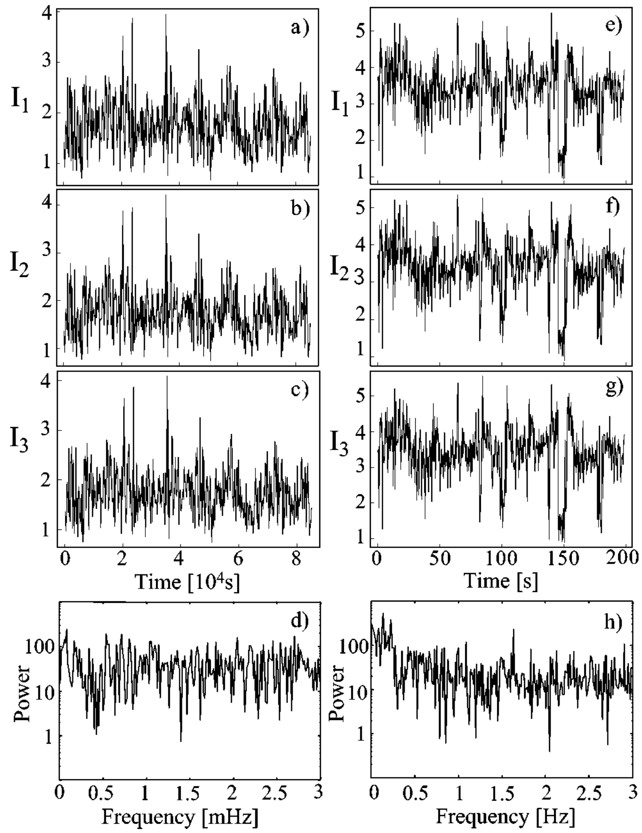

FIG. 6. (a,b,c) Amplitudes I_i of the three peaks composing the hexagonal pattern as a function of time, for $\Omega=3$, $\varepsilon=0.003$, and $\delta t=200$ s. (e,f,g) Same as (a)–(c), with $\delta t=0.39$ s. (d,h) Mean temporal Fourier transform of the above I_i ($i=1,2,3$) for $\delta t=200$ s and $\delta t=0.39$ s, respectively, in a semilogarithmic scale. In all the figures, arbitrary units have been used on the y axis.

consisting of rolls appear in the hexagonal pattern. These small domains are randomly distributed. Their number depends on ε, and is independent of Ω. Secondly, the hexagonal pattern is progressively invaded from the cell edge towards the center by three different sets of rolls. These three

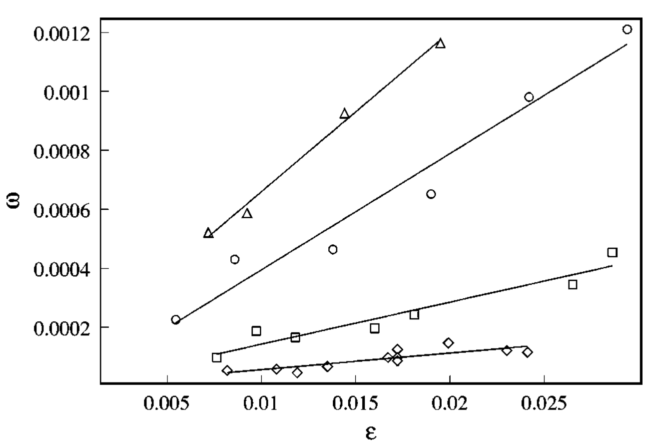

FIG. 7. Dimensionless rotation frequency ω of the 2D Fourier transform as a function of ε, for $\Omega=2$ ($\diamond$), $\Omega=3$ ($\square$), $\Omega=4.2$ ($\bigcirc$), and $\Omega=5$ ($\triangle$). The solid lines represent the best linear fit for each Ω series: $\omega=a_\Omega\varepsilon$.

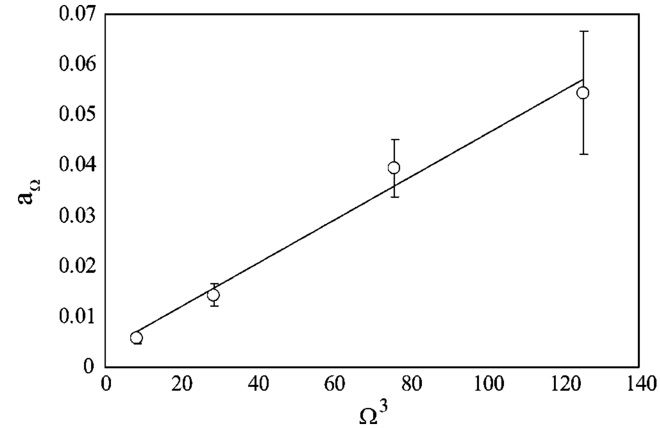

FIG. 8. The coefficient a_Ω as a function of Ω^3. The straight line represents the best linear fit ($a_\Omega=m\Omega^3$). The coefficient of linear correlation is 0.99 and $m=4.6\times10^{-4}$.

sets of rolls appear at a lower ε when Ω increases. For $\Omega<3$, the interval in ε in which the hexagonal pattern, and then the rolls, predicted by the bifurcation diagram in the nonrotating case develop (Fig. 1), becomes smaller for large rotation rates. For $3\leqslant\Omega\leqslant6$, the system switches directly from the hexagonal pattern to the three sets of rolls, and the rolls predicted for large ε never develop. For $\Omega\geqslant6$, the hexagonal pattern is never observed and the three sets of rolls develop at the onset of convection. These results are summarized in the experimental phase diagram in Fig. 4. The two-dimensional Fourier transform always displays three peaks, characteristic of the hexagonal pattern as well as three differently oriented sets of rolls.

For any rotation rate Ω, we have observed a slow rotation of the convective pattern, in the direction opposite to the rotation cell (ω in the rotating frame). The pattern therefore

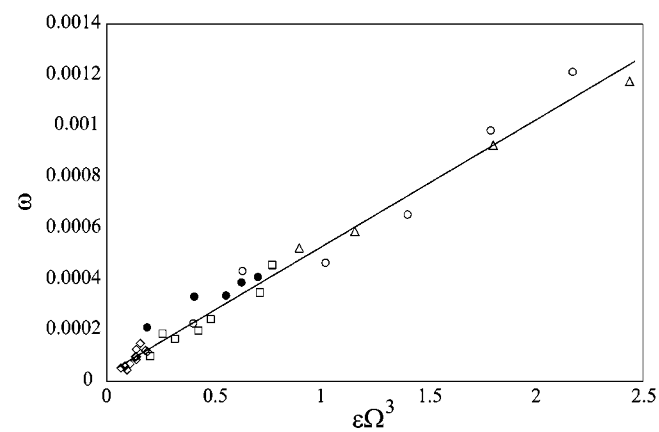

FIG. 9. Dimensionless rotation frequency ω as a function of $\varepsilon\Omega^3$. The solid circles represent the measurements made at $\Omega=3.93$ with the cell for which the bottom plate is shaped with a cosinusoidal ramp. The other series of points are defined in Fig. 7. The different Ω-series points collapse together on a single curve. The solid line represents the best linear fit ($\omega=c\varepsilon\Omega^3$). We find $c=4.6\times10^{-4}$, which is in agreement with the fit of Fig. 8.

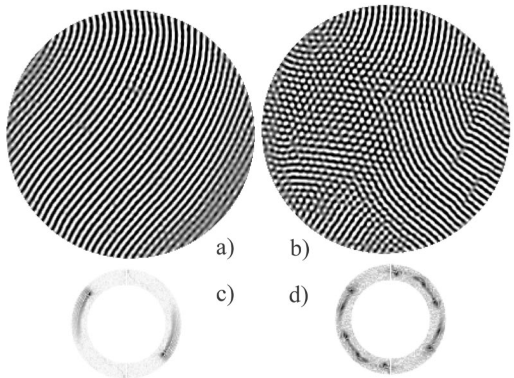

FIG. 10. (a,b) Images of the convective pattern (observed from above) in the cell with a ramp on the bottom plate, for $\varepsilon=0.012$ and $\varepsilon=0.046$, respectively. In both experiments, $\Omega=3.93$. (c,d) Structure functions associated with (a) and (b), respectively. Image processing has been required to obtain these pictures (see text).

rotates slower than the cell. ω is found to depend both on Ω and ε, and to follow $\omega=c\varepsilon\Omega^3$, with $c=4.6\times10^{-4}$. This relationship does not depend on the boundary conditions or the thickness of the cell.

Our experimental results seem to confirm that, in order to make good predictions, a theoretical model must take in account the spatial modulation [23,24], rather than simply mode interactions [20–22]. Indeed, mode interaction models predict the onset of oscillating hexagons via a Hopf bifurcation, and do not allow the possibility of the pattern defects observed in our experiments. In order to make a more quantitative comparison with the spatially and temporally modulated hexagons predicted by [23,24], further experiments are necessary.

ACKNOWLEDGMENTS

All experiments have been performed at iQuest, in the laboratory of Guenter Ahlers: we are grateful to him for providing all the apparatus and making this work possible. We also wish to thank Hermann Riecke for the interesting discussions about this work, and Sergio Ciliberto for his valuable help.

[1] H. Bénard, Rev. Gen. Sci. Pures Appl. **11**, 1261 (1900); Ann. Chim. Phys. **23**, 62 (1901).
[2] A large literature pertaining to this field has evolved. Particulary useful as introductions to early work are the reviews by E. L. Kosscmieder and E. L. Koschmieder in Adv. Chem. Phys. **26**, 177 (1974), and in *Order and Fluctuations in Equilibrium and Nonequilibrium Statistical Mechanics*, XVI International Solvay Conference, edited by G. Nicolis, G. Dewel, and J. W. Turner (Wiley, New York, 1981), p. 169; by F. Busse, in *Hydrodynamic Instabilities and the Transition to Turbulence*, edited by H. L. Swinney and J. P. Gollub (Springer, Berlin, 1981), p. 97; in Rep. Prog. Phys. **41**, 1929 (1978); and by R.P. Behringerin, Rev. Mod. Phys. **57**, 657 (1985).
[3] E. Bodenschatz, W. Pesch, and G. Ahlers, Annu. Rev. Fluid Mech. **32**, 709 (2000).
[4] A. Oberbeck, Annu. Rev. Phys. Chem. **7**, 271 (1879).
[5] J. Boussinesq, *Théorie Analytique de la Chaleur* (Gauthier-Villars, Paris, 1903), Vol. 2.
[6] E. Palm, J. Fluid Mech. **8**, 183 (1960).
[7] L. A. Segel and J. T. Stuart, J. Fluid Mech. **13**, 289 (1962).
[8] F. H. Busse, J. Fluid Mech. **30**, 625 (1967).
[9] E. Palm, T. Ellingsen, and B. Gjerik, J. Fluid Mech. **30**, 651 (1967).
[10] S. H. Davis and L. A. Segel, Phys. Fluids **11**, 478 (1968).
[11] F. H. Busse, in *Mantle Convection, Plate Tectonics and Global Dynamics*, edited by W. R. Peltier, Vol. 4 of *The Fluid Mechanics of Astrophysics and Geophysics* (Gordon and Breach, New York, 1989).
[12] C. Q. Hoard, C. R. Robertson, and A. Acrivos, Int. J. Heat Mass Transfer **13**, 849 (1970).
[13] M. Dubois, P. Bergé, and J. Wesfried, J. Phys. (France) **39**, 1253 (1978).
[14] R. W. Walden and G. Ahlers, J. Fluid Mech. **109**, 89 (1981).
[15] S. Ciliberto, E. Pampaloni, and C. Pérez-García, Phys. Rev. Lett. **61**, 1198 (1988).
[16] S. Ciliberto, P. Coullet, J. Lega, E. Pampaloni, and C. Pérez-García, Phys. Rev. Lett. **65**, 2370 (1990).
[17] E. Bodenschatz, J. R. de Bruyn, G. Ahlers, and D. S. Cannell, Bull. Am. Phys. Soc. **36**, 653 (1991).
[18] E. Bodenschatz, J. R. de Bruyn, G. Ahlers, and D. S. Cannell, Phys. Rev. Lett. **67**, 3078 (1991).
[19] G. Küppers and D. Lortz, J. Fluid Mech. **35**, 609 (1969).G. Küppers, Phys. Lett. **32A**, 7 (1970).
[20] B. Echebarria and H. Riecke, Physica D **139**, 97 (2000).
[21] J. Swift, in *Contemporany Mathematics* (American Mathematical Society, Providence, 1984), Vol. 28.
[22] A. Soward, Physica D **14**, 227 (1985).
[23] F. Sain and H. Riecke, Physica D **144**, 124 (2000).
[24] B. Echebarria and H. Riecke, Phys. Rev. Lett. **84**, 4838 (2000).
[25] J. R. deBruyn, E. Bodenschatz, S. Morris, S. Trainoff, Y.-C. Hu, D. S. Cannel, and G. Ahlers, Rev. Sci. Instrum. **67**, 2943 (1996).
[26] The diamond machine was done by Laser Power Optics, 12777 High Bluff Drive, San Diego, CA 92130.